

# Optical tweezing using tunable optical lattices along a silicon nanobeam waveguide:

## Supplementary Information

C. Pin,<sup>a,b</sup>†‡ J.-B. Jager,<sup>b</sup> M. Tardif,<sup>b</sup> E. Picard,<sup>b</sup> E. Hadji,<sup>b</sup> F. de Fornel,<sup>a</sup> B. Cluzel<sup>a\*</sup>

<sup>a</sup>Groupe Optique de Champ Proche, Laboratoire Interdisciplinaire Carnot de Bourgogne UMR CNRS  
6303, Université de Bourgogne Franche-Comté, 21078 Dijon, France.

<sup>b</sup>Univ. Grenoble Alpes, CEA, INAC, PHELIQS, SINAPS, F-38000 Grenoble, France.

*\*Corresponding author: Benoît Cluzel, [benoit.cluzel@u-bourgogne.fr](mailto:benoit.cluzel@u-bourgogne.fr)*

*†Present address: Research Institute for Electronic Science, Hokkaido University,  
Sapporo, Hokkaido, 001-0020, Japan.*

*‡ORCID iD: 0000-0002-5088-5711*

## Supplementary Movies:

### Movie S1: Optical trapping using tunable optical lattices on a silicon chip.

Part 1: 500 nm fluorescent polystyrene beads trapped in a TE<sub>0</sub>-TE<sub>1</sub> lattice

(wavelength: 1530 nm, source power: 224 mW, duration: 10 s)

Part 2: 500 nm fluorescent polystyrene beads trapped in a TM<sub>0</sub>-TE<sub>1</sub> lattice

(wavelength: 1530 nm, source power: 224 mW, duration: 10 s)

Part 3: 1 μm fluorescent polystyrene beads trapped in a TM<sub>0</sub>-TE<sub>1</sub> lattice

(wavelength: 1530 nm, source power: 224 mW, duration: 10 s)

Part 4: *E. Coli* bacteria trapped in a TM<sub>0</sub>-TE<sub>1</sub> lattice

(wavelength: 1550 nm, source power: 100 mW, duration: 17 s)

### Movie S2: Optical manipulation using tunable optical lattices on a silicon chip.

Part 1: Cascade displacement of 1 μm fluorescent polystyrene beads trapped in a TM<sub>0</sub>-TE<sub>1</sub> lattice

(wavelength: 1530 nm, source power: 224 mW, duration: 11 s, scale bar: 5 μm)

Part 2: Demonstration of on-demand transport of 1 μm fluorescent polystyrene beads trapped in a TM<sub>0</sub>-TE<sub>1</sub> lattice (wavelength: 1530 nm, source power: 224 mW, duration: 49 s, scale bar: 5 μm)

Part 3: Demonstration of the lattice period tunability with 1 μm fluorescent polystyrene beads trapped in a TM<sub>0</sub>-TE<sub>1</sub> lattice (wavelength: 1530 – 1537.5 – 1545 – 1552.5 – 1560 nm, source power: 224 mW, duration: 87 s, scale bar: 5 μm)

Part 4: Demonstration of an on-chip tractor beam acting on 500 nm fluorescent polystyrene beads trapped in a TM<sub>0</sub>-TE<sub>1</sub> lattice (wavelength: 1530 ~ 1545 nm, source power: 200 mW, duration: 19 s, scale bar: 5 μm)

## Supplementary Information:

### 1. Influence of the waveguide's width and the laser wavelength on the near-field mode-beating period

The waveguide's width and the laser wavelength are both parameters influencing the propagation constant of the guided modes. Fig. S1a and S1b show the variation of the effective refractive indices of the three guided modes considered in this work as a function of both these parameters, respectively. As mentioned in the main text, effective index values were obtained from Finite-Element Method numerical simulations. The variation of the effective indices directly impacts the near-field mode-beating period. Fig. S1c and S1d show the variation of the periods of the three different near-field mode-beating configurations represented in Fig. 1(c). Period values were calculated using the equation (1) introduced in the main text.

As indicated by the red dotted vertical lines in Fig. S1a and S1c, using a 510 nm waveguide's width allows for the propagation of the first order TE mode ( $TE_1$ ), while still keeping its effective index as low as possible, close to the value of the refractive index of silica. The  $TE_0$ - $TE_1$  and  $TM_0$ - $TE_1$  mode-beating period is thus minimized, which is of prime importance in order to create optical traps, especially in the case of the  $TM_0$ - $TE_1$  lattice. Indeed, the gradient of the effective near-field intensity's periodic patterns (see Fig. 1(c)) has to be strong enough along the waveguide axis for the resulting gradient force to balance the scattering force, and thus achieve an equilibrium state.

It can be also seen in Fig. S1b that a variation of wavelength has less impact on the effective index of the near-cutoff  $TE_1$  mode than on the effective indices of the two fundamental modes. As explained in the article, this difference enables controlling the near-field mode-beating period by modifying the laser wavelength. The spectral tunability of the lattice period is especially pronounced in the case of the  $TM_0$ - $TE_1$  lattice.

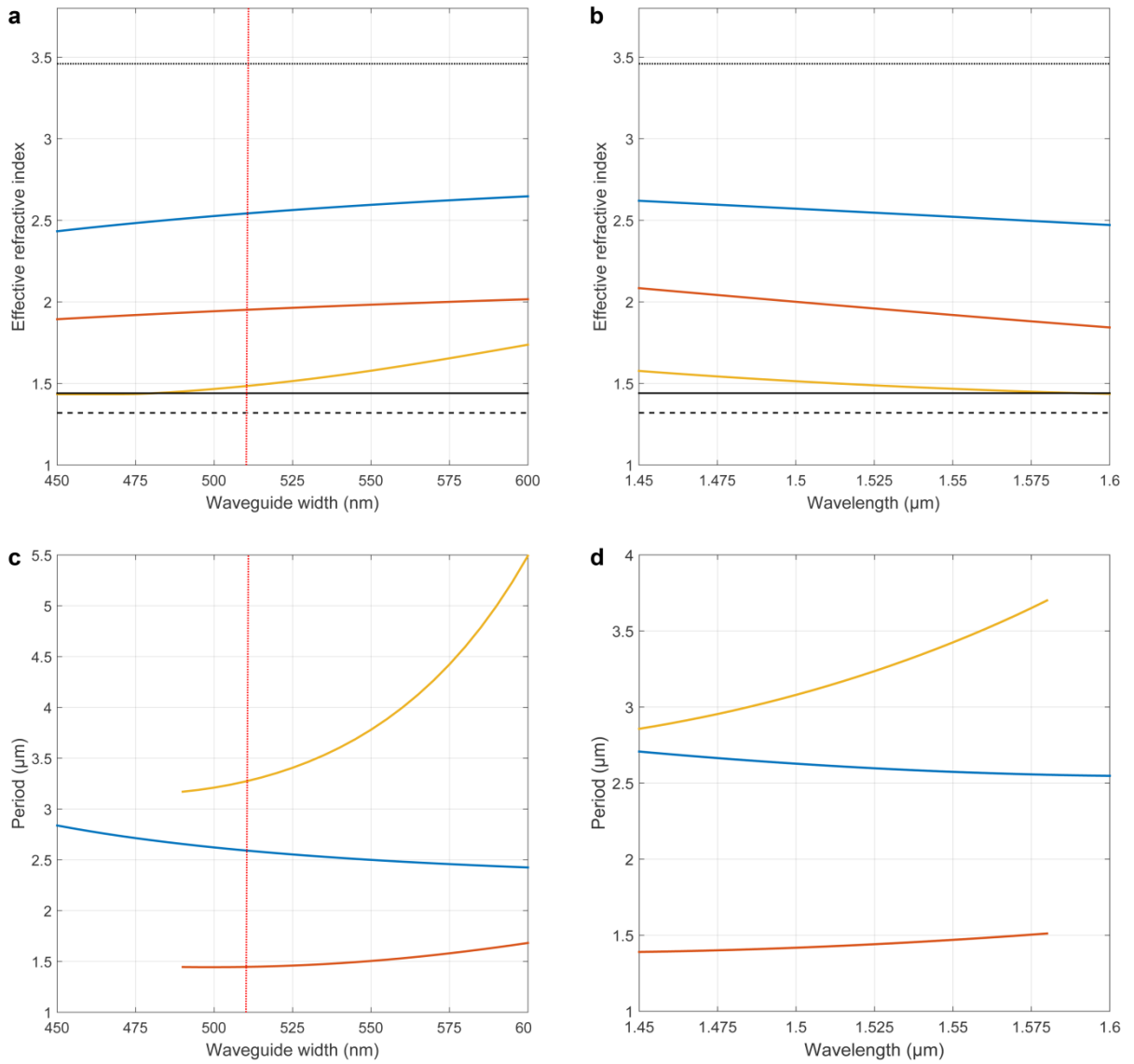


**Fig. S1.** Effective indices and near-field mode-beating periods. (a,b) Effective refractive indices of the three different propagating modes considered in this work (blue curve:  $TE_0$ , red curve:  $TM_0$ , orange curve:  $TE_1$ ) as a function of (a) the waveguide's width at a wavelength of 1530 nm, and (b) the laser wavelength in the case of a 510-nm-large waveguide. Refractive indices of silica, silicon and water are respectively indicated by the black solid, dotted and dashed lines. (c,d) Periods of the three mode-beating patterns depicted in Fig. 1c (blue curve:  $TE_0$ - $TM_0$ , red curve:  $TE_0$ - $TE_1$ , orange curve:  $TM_0$ - $TE_1$ ) as a function of (c) the waveguide's width at a wavelength of 1530 nm, and (d) the laser wavelength in the case of a 510-nm-large waveguide. Red dotted lines correspond to the 510-nm-large waveguide geometry used in this work.

## 2. Spatial distribution of the TE<sub>0</sub>-TM<sub>0</sub> mode beating pattern

As mentioned in the article, when both TE<sub>0</sub> and TM<sub>0</sub> fundamental modes co-propagate in the waveguide, near-field mode beating induces a slight lateral undulation of the top-surface effective near-field intensity along the waveguide. This effect is evidenced in Fig. S2 where are plotted multiple cross-sections of the effective intensity taken at different distance along a one-period-long portion of waveguide. As can be seen, the position of the effective near-field intensity above the top surface oscillates alternatively from one side to the other side of the waveguide. However, no local attenuation or enhancement of the effective intensity can be noted. As a consequence, particles are still propelled above the top surface of the waveguide, meandering periodically as it was first observed and reported by Tanaka and Yamamoto (10).

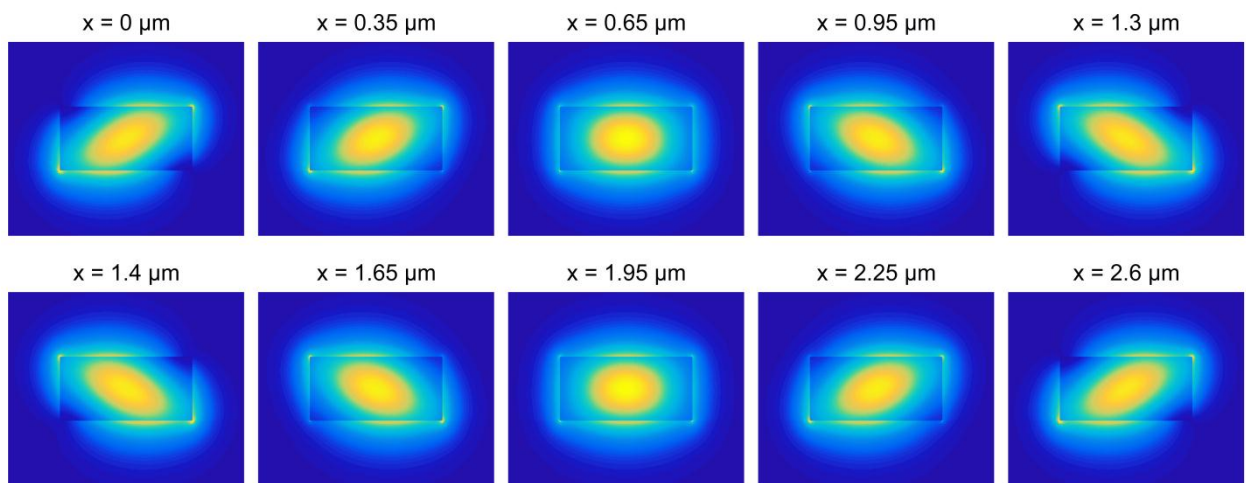


**Fig. S2.** Near-field mode beating between the TE<sub>0</sub> and TM<sub>0</sub> modes. Successive cross-sections showing the variation of the effective intensity resulting from the co-propagation of the TE<sub>0</sub> and TM<sub>0</sub> modes along a one-period-long portion of a 510-nm-large waveguide.

### 3. Stable optical trapping using a $\text{TM}_0\text{-TE}_1$ lattice

The  $\text{TM}_0\text{-TE}_1$  lattice was found to be particularly efficient for optical trapping of 1  $\mu\text{m}$  beads, allowing for stable trapping over long periods of time. Fig. S3 shows the kymograph of an experiment where 1  $\mu\text{m}$  beads were stably trapped for several minutes. Using a particle tracking technique described in previously published work (30), histograms of trapped particles' positions were plotted in order to obtain two-dimensional maps of the trapping potentials experienced by these beads. Data obtained for two different beads are plotted in Fig. S4. Experiments with 500 nm beads led to similar observations, although perturbations due to multiple particle trapping resulted in faster bead propagation from trap to trap, as it can be seen in Fig. S5. Yet, tracking the position of single particles stably trapped for about 45 s without any external perturbation made it possible to plot two-dimensional maps of the trapping potentials experienced by these beads, as shown in Fig. S6.

In both 500 nm and 1  $\mu\text{m}$  beads' cases, trapping potential wells with elongated shape were obtained. This asymmetric shape results in the traps being stiffer along the lateral direction than along the waveguide axis. The cause of the slightly curved shape of the trapping potential wells plotted in Fig. S4 and Fig. S6 can be attributed to the undesired excitation of the  $\text{TE}_0$  mode, yet in a weaker extent compared with the  $\text{TM}_0$  and  $\text{TE}_1$  modes. The slight undulation that is observed is consistent with the  $\text{TE}_0\text{-TM}_0$  near-field mode-beating pattern described in the previous section.

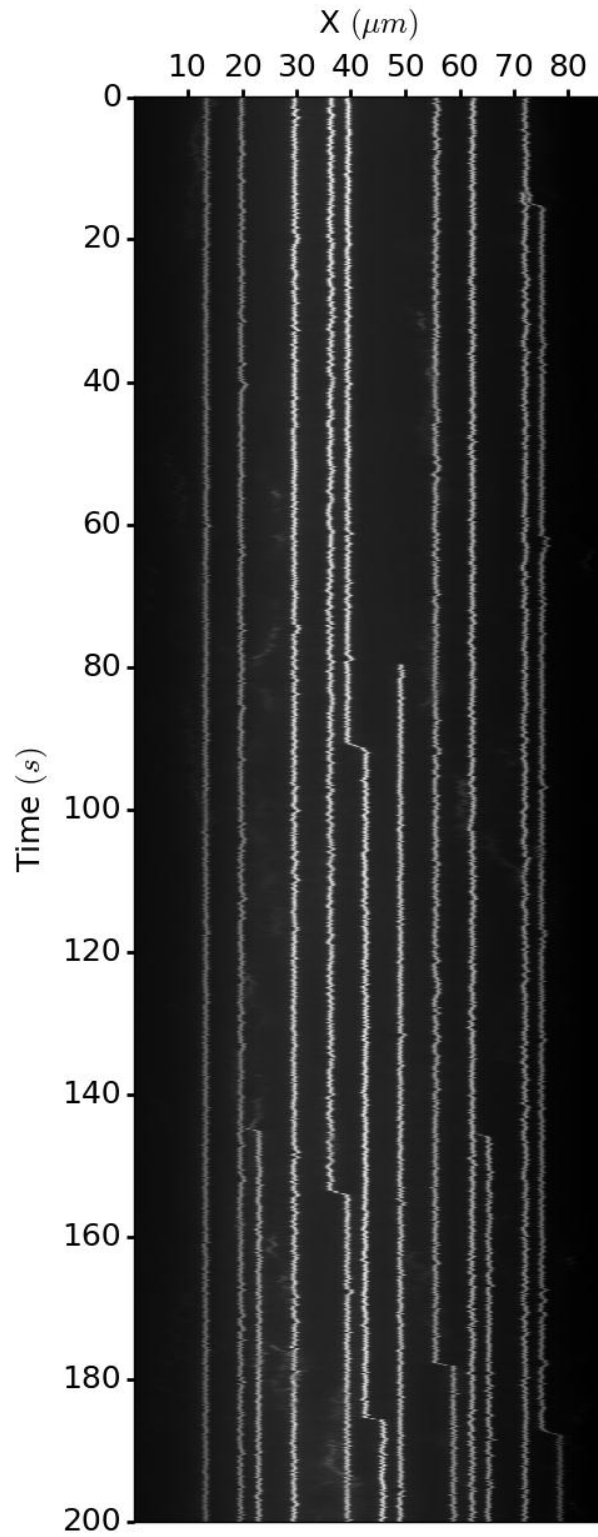


**Fig. S3.** Stable trapping of 1  $\mu\text{m}$  beads in a  $\text{TM}_0\text{-TE}_1$  lattice. Kymograph showing the time evolution of the positions of 1  $\mu\text{m}$  beads trapped in a  $\text{TM}_0\text{-TE}_1$  lattice. The laser wavelength and power used for this experiment were respectively 1530 nm and 224 mW after laser light amplification.

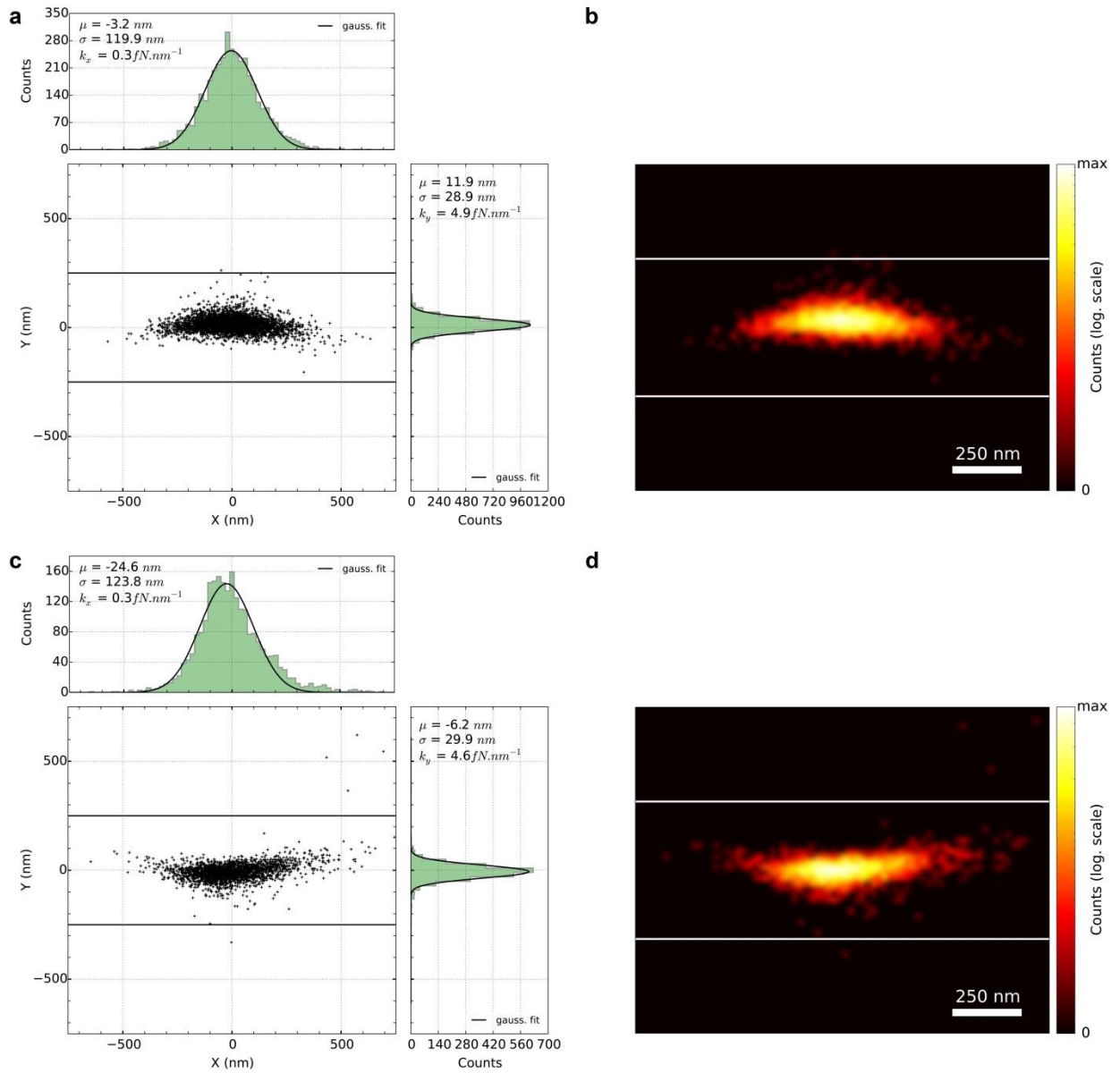


**Fig. S4.** Trapping potentials experienced by 1  $\mu\text{m}$  beads in  $\text{TM}_0\text{-TE}_1$  lattice. Two-dimensional plots of trapped particles' positions and experimental maps of the trapping potentials experienced by two different 1  $\mu\text{m}$  beads trapped in the  $\text{TM}_0\text{-TE}_1$  lattice shown in Fig. S3.

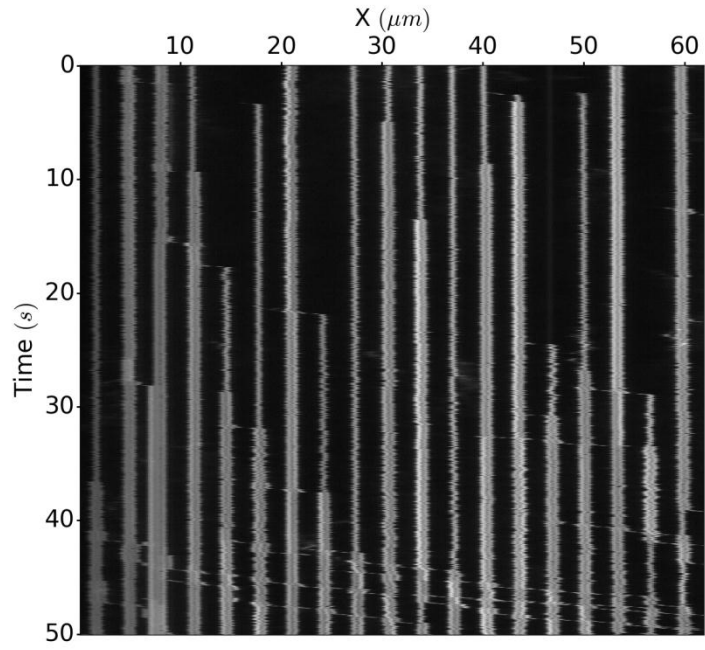


**Fig. S5.** Stable trapping of 500 nm beads in a  $TM_0$ - $TE_1$  lattice. Kymograph showing the time evolution of the positions of 500 nm beads trapped in a  $TM_0$ - $TE_1$  lattice. The laser wavelength and power used for this experiment were respectively 1530 nm and 158 mW after laser light amplification.

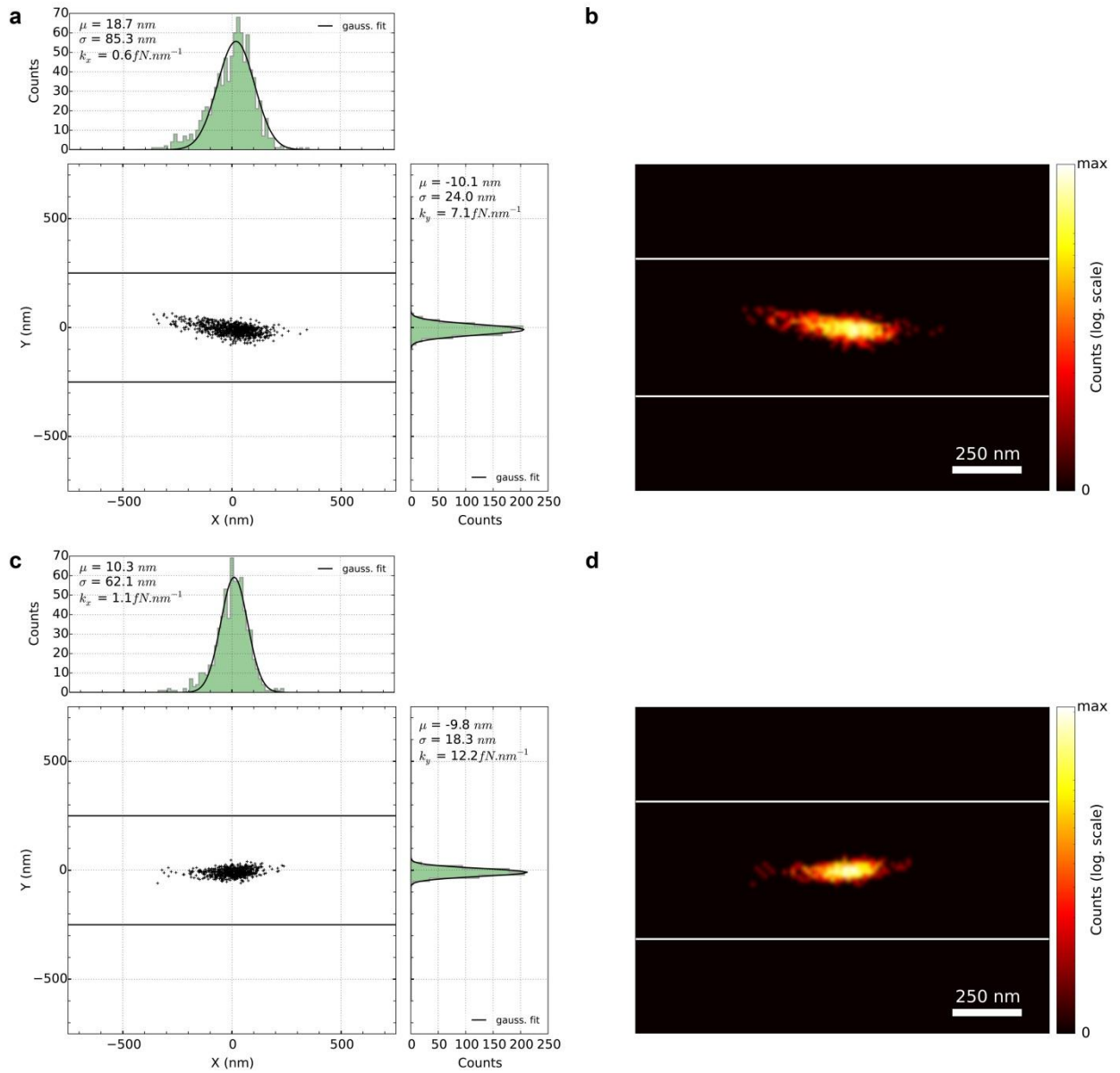


**Fig. S6.** Trapping potentials experienced by 500 nm beads in  $\text{TM}_0\text{-TE}_1$  lattice. Two-dimensional plots of trapped particles' positions and experimental maps of the trapping potentials experienced by two different 500 nm beads trapped in the  $\text{TM}_0\text{-TE}_1$  lattice shown in Fig. S5.

#### 4. Fast wavelength scanning for the modulation of the trapped particles' velocity

As a complement to the optical manipulation techniques presented in Fig. 5, the kymograph presented in Fig. S7 shows the behaviour of 500 nm beads propelled on a waveguide while quickly and repeatedly scanning the laser wavelength in order to induce a fast back-and-forth motion of the  $\text{TM}_0\text{-TE}_1$  lattice's traps. Due to the fast modulation of the wavelength and because of the viscous drag effect in water, the beads are unable to follow the repeated displacements of the traps. Instead, an average propelling force is applied to the beads, the intensity of which differs depending on whether the wavelength increases or decreases, hence on the direction of the traps' displacements. As can be seen in Fig. S7, the mean velocity of the trapped particles is indeed periodically modulated, being slower when the wavelength decreases. When the wavelength decreases, the lattice shrinks, which leads to the traps' displacements and the beads' motion being in opposite directions. On the contrary, the particles' velocity appears to be faster during the phases of lattice expansion, when the traps are displaced forward, in the same direction as the beads' motion. This result denotes that dynamic control of the laser wavelength might be also advantageously used to control the velocity of the particles being optically trapped and manipulated using near-field mode-beating lattices, without loosening the orthogonal trap stiffness by decreasing the laser power.

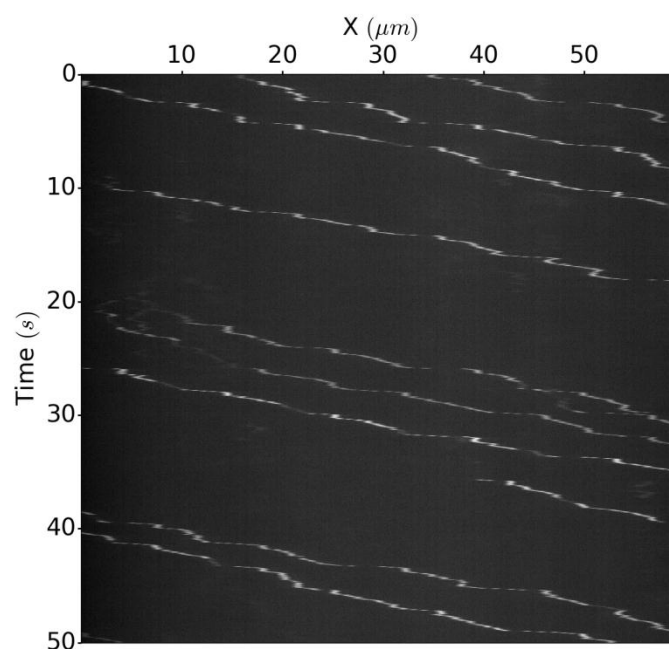


**Fig. S7.** Modulation of the trapped particles' velocity via fast wavelength scanning. Kymograph showing the time evolution of the position of 500 nm beads trapped in a  $\text{TM}_0\text{-TE}_1$  lattice while the laser wavelength is repeatedly scanned from 1530 nm to 1565 nm and back again to 1530 nm. The laser power used for this experiment was 200 mW after laser light amplification.